



1 Internal tree cycling and atmospheric archiving of mercury: examination 2 with concentration and stable isotope analyses.

3 David S. McLagan^{1,2,3}, Harald Biester¹, Tomas Navrátil⁴, Stephan M. Kraemer⁵, Lorenz
4 Schwab^{5,6}

5 ¹Institute of Geoecology, Technical University of Braunschweig, Braunschweig, 38106, Germany

6 ²Dept. of Physical and Environmental Sciences, University of Toronto Scarborough, M1C1A4
7 Canada

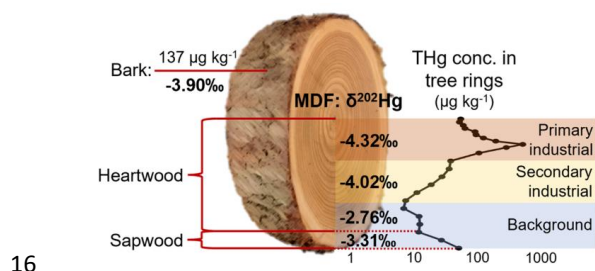
8 ³School of Environmental Studies and Dept. of Geological Sciences and Geological Engineering,
9 Queen's University, K7L3N6 Canada

10 ⁴Institute of Geology of the Czech Academy of Sciences, Prague, 117 20, Czech Republic

11 ⁵Department for Environmental Geochemistry, Centre for Microbiology and Environmental
12 Systems Science, University of Vienna, Vienna, 1090, Austria

13 ⁶Doctoral School in Microbiology and Environmental Science, University of Vienna, Vienna, 1090,
14 Austria

15 Correspondence to: david.s.mclagan@gmail.com



16
17 **Abstract.** Trees predominantly take up mercury (Hg) from the atmosphere via stomatal assimilation
18 of gaseous elemental Hg (GEM). Hg is oxidised in leaves/needles and transported to other tree
19 anatomy including bole wood where it can be stored long-term. Using Hg archived with growth
20 rings facilitates archiving of historical GEM concentrations. Nonetheless, there are significant
21 knowledge gaps on the cycling of Hg within trees. We investigate Hg archived in tree rings, internal
22 tree Hg cycling, and differences in Hg uptake mechanisms in Norway spruce and European larch
23 sampled within 1 km of a HgCl₂ contaminated site using total Hg (THg) and Hg stable isotope



24 analyses. Tree ring samples are indicative of significant increases in THg concentrations (up to
25 $521\mu\text{g}\cdot\text{kg}^{-1}$) from *background period* (BGP; facility closed; 1992—present) to *secondary industrial*
26 *period* (2ndIP; no HgCl₂ wood treatment; 1962–1992) to *primary industrial period* (1stIP; active
27 HgCl₂ wood treatment; \approx 1900–1962). Mass dependent fractionation (MDF) Hg stable isotope data
28 are shifted negative during industrial periods ($\delta^{202}\text{Hg}$: 1stIP: $-4.32\pm 0.15\%$; 2ndIP: $-4.04\pm 0.32\%$;
29 BGP: $-2.83\pm 0.74\%$; 1SD). Even accounting for a \approx -2.6‰ MDF shift associated with stomatal uptake,
30 these data are indicative of emissions derived from industrial activity being enriched in lighter
31 isotopes associated with HgCl₂ reduction and Hg⁰ volatilisation. Similar MDF ($\delta^{202}\text{Hg}$: $-3.90\pm 0.30\%$;
32 1SD) in bark Hg ($137\pm 105\mu\text{g}\cdot\text{kg}^{-1}$) suggests that stomatal assimilation and downward transport is
33 also the dominant uptake mechanism for bark Hg (reflective of negative stomatal uptake MDF shift)
34 rather than deposition to bark. THg was enriched in sapwood of all sampled trees across both tree
35 species. This may indicate long-term storage of a fraction of Hg in sapwood or xylem solution. These
36 data advance our understanding of the physiological processing of Hg within trees and provide critical
37 direction to future research into the use of trees as archives for historical atmospheric Hg.

38 Key words

39 Mercury biogeochemistry, tree rings, sapwood (hydroactive xylem), heartwood, phloem, bark,
40 process and source tracing.

41 1. Introduction

42 Until the last 10—15 years, it was hypothesised that the major transfer pathway of mercury (Hg)
43 from the atmospheric to terrestrial and aquatic matrices was the wet and dry deposition of Hg(II) as
44 either gaseous oxidised Hg (GOM) or particulate bound-Hg (PBM) (Lin and Pehkonen, 1999;
45 Lindberg et al., 2007; Selin, 2009). However, studies began to suggest that dry deposition of gaseous
46 elemental Hg (GEM) had to be more important than was thought because of inconsistencies between
47 measurement data of atmospheric Hg species and modelling predictions (Selin et al., 2008; Zhang et
48 al., 2009; Mao and Talbot, 2009). A major mechanism for dry deposition of GEM is uptake and
49 assimilation to flora via stomata during plant respiration, an idea that was posited by scientists as far
50 back as the late 1970s (Browne and Fang, 1978; Lindberg et al., 1979). The rate of GEM uptake
51 correlates to photosynthetic activity of the plants (Laacouri et al., 2013), but is also species dependent
52 since it is related to stomatal conductance and the number of stomata per leaf (Laacouri et al., 2013;
53 Millhollen et al., 2006). Recent work has provided evidence that dry deposition of GEM to vegetation
54 via stomatal uptake and subsequent transfer via leaf/needle senescence, abscission, and litterfall is



55 likely to be the dominant mechanism for Hg deposition from the atmosphere to terrestrial matrices
56 (Obrist et al., 2017; 2018; Jiskra et al., 2018).

57 Similarly, there is strong evidence that GEM is also the major source of Hg in bole wood (Scanlon
58 et al, 2020, Wang et al., 2020; 2021). Using Hg stable isotope measurements, GEM deposition has
59 been estimated to supply 57–94 % of total Hg (THg) in vegetated terrestrial systems (Khan et al.,
60 2019 and references therein). A major loss mechanism of Hg from forest ecosystems is during
61 biomass burning (Friedli et al., 2009; McLagan et al., 2021a; Dastoor et al., 2022).

62 To assess Hg cycling within trees we must also reflect on alternative uptake mechanisms: (i) uptake
63 from roots and (ii) deposition to above ground tree surfaces (stems, leaves, and bark) and potential
64 sorption to and translocation into tree tissue. Hg uptake from roots has been studied for decades. Data
65 overwhelmingly show minimal transport of Hg from the root zone to aerial mass of trees (Beauford
66 et al., 1977; Lindberg et al., 1979; Bishop et al., 1998; Moreno et al., 2005; Graydon et al. 2009; Cui
67 et al., 2014; Cozzolino et al., 2016; Peckham et al., 2019a). Even in soils with elevated THg
68 concentrations, upward transfer from roots is low in relative terms (Beauford et al., 1977; Lindberg
69 et al., 1979; Graydon et al. 2009). Limited uptake of Hg and other metals via the roots has been
70 attributed to restrictive barriers in the roots such as that provided by the endodermis (Kahle, 1993).
71 Alternatively, Hg can also be deposited to surfaces of the aerial anatomy of trees, predominantly as
72 GOM and PBM (Rea et al., 2002; Mowat et al., 2011; Laacouri et al., 2013). Hg on leaf surfaces
73 contributes only a minor fraction of THg in foliage and accumulation rates are low due to both
74 precipitation wash-off (Rea et al., 2000; 2001; Laccouri et al., 2013) and photoreduction and
75 subsequent evasion of GEM (Graydon et al., 2006; Mowat et al., 2011). Several studies have
76 demonstrated elevated bark THg concentrations relative to branch and bole wood (Siwik et al., 2010;
77 Zhou et al., 2017; Liu et al., 2020). Therefore, it has been suggested that Hg in bark is chiefly derived
78 from atmospheric deposition (Chiarantini et al., 2016; 2017) potentially with a greater proportion of
79 GOM and PBM rather than GEM (Peckham et al., 2019a).

80 Trees make up a large sink for atmospheric Hg and therefore play an important role in the global
81 Hg cycle. Hg has no known biological function in plants (Moreno-Jiménez et al., 2006; Peralta-Videa
82 et al., 2009; Cozzolino et al., 2016); thus, it is important to understand the physiological processing
83 of Hg within trees from a phytotoxicological standpoint. After assimilation through leaf/needle stoma
84 GEM is assumed to be oxidised to form Hg(II) compounds and integrate with internal leaf tissue
85 (Laacouri et al., 2013; Demers et al., 2013). A recent study examining three evergreen species used
86 Hg stable isotopes to show that reduction and re-release can occur (Yuan et al., 2018). Although the
87 bole wood of trees has lower THg concentrations than bark and needles/leaves in both deciduous and



88 evergreen species (Navrátil et al., 2017; Zhou et al., 2017; Liu et al., 2020), the overall Hg loading
89 of the tree is the reverse: wood carries the largest total mass of Hg due to much greater overall biomass
90 (Liu et al., 2020).

91 Hg is transported from the foliage to bole wood via the phloem, which is the conduit for nutrient
92 and photosynthetic product transfer from leaves/needles to the rest of the trees (Cutter and Guyette,
93 1993). Phloem lies between the cambium (tissue that promotes new xylem and phloem growth) and
94 the inner bark. Once oxidised to Hg(II) species in the leaves/needles, it likely associates with
95 phytochelatin, cysteine compounds for phloem transport (O'Connor et al., 2019; Dennis et al., 2019).
96 Phloem-to-xylem translocation (new xylem makes up sapwood and forms tree rings) is expected to
97 occur throughout this downward transport (Arnold et al., 2018; Yanai et al., 2020; Nováková et al.,
98 2021; 2022). This translocation likely proceeds via *rays*, parenchyma cells that radially connect xylem
99 and phloem conductive tissues and mediate water and nutrient transport, tree growth, and biotic and
100 abiotic stressors (Nagy et al., 2014; Pfautsch et al., 2015; Gustin et al., 2022). THg is expected to be
101 preserved in the newly forming xylem tree rings; and hence, THg concentrations in tree rings have
102 been used as a proxy for historical atmospheric GEM concentration (Siwik et al., 2010; Wright et al.,
103 2014; Clackett et al., 2018). This includes identification of elevated GEM concentrations, past and
104 present, associated with atmospheric Hg emissions from industrial activities located near sampled
105 trees (Odabasi et al., 2016; Navrátil et al., 2017; Scanlon et al., 2020; Nováková et al., 2022). A
106 potential caveat to this method of chronicling historical atmospheric GEM concentrations is the
107 translocation of Hg between tree rings that has been reported in certain studies; tree ring
108 concentrations do not reflect reported industrial activity (Nováková et al., 2021; Wang et al., 2021).
109 However, there are a number of studies that demonstrate this inter-ring translocation does not
110 significantly influence results; tree ring Hg concentrations reflect reported industrial (Clackett et al.,
111 2018; Navrátil et al., 2018; Peckham et al., 2019b). Tree species may be a factor affecting inter-ring
112 Hg translocation (Scanlon et al., 2020; Nováková et al., 2021).

113 Hg stable isotopes represent a powerful and relatively new technique that can provide information
114 relating to the biogeochemical cycling history and potentially source information of sampled Hg
115 (Bergquist and Bloom 2007; 2009). This premise assumes distinct “signature” ratios of different
116 sources, and mass-dependant (MDF) and mass-independent (MIF) fractionations of the seven stable
117 Hg isotopes that can be imparted by environmental transformation processes (Bergquist and Bloom
118 2007; 2009). Forest ecosystems are no exception to this. For instance, Hg stable isotopes added
119 substantial evidence to the argument that GEM stomatal assimilation and eventual litterfall (or
120 vegetation death) was the dominant mechanism for Hg deposition to soils in vegetated ecosystems



121 (Wang et al., 2017; Jiskra et al., 2018; Yuan et al., 2018). Studies examining Hg stable isotopes in
122 tree-rings are limited (Scanlon et al., 2020; Wang et al., 2021). Both studies associated differences in
123 MIF ($\Delta^{199}\text{Hg}$) with varying sources over time, but Wang et al. (2021) suggested there were limitations
124 to this interpretation due to inter-ring translocation of Hg. They also attribute differences in MDF
125 ($\delta^{202}\text{Hg}$) with physiological differences (i.e., inter-ring translocation, stomatal conductance, and
126 canopy dynamics), particularly as they relate to tree species, and environmental factors (i.e., soil
127 conditions, slope, and winds) (Wang et al., 2021).

128 In this study, we examine THg concentrations and stable isotopes in two coniferous tree species,
129 Norway spruce (*Picea abies*) and European larch (*Larix decidua*), surrounding a legacy Hg
130 contaminated site in the German Black Forest. We aim to investigate if historical records of the
131 industrial activities correlate with elevated THg concentrations in tree rings of sampled trees. There
132 are no records of historical atmospheric Hg emissions or concentrations at this site, which was subject
133 primarily to soil and water contamination (application of low-volatility HgCl_2 solution) rather than
134 combustion emissions to the atmosphere. Thus, we compliment tree-ring data with deployments of
135 GEM passive air samplers (PASs) at the site to assess atmospheric GEM conditions at the former
136 industrial site past (tree rings) and present (PASs). Using Hg stable isotopes, we aim to examine
137 potential source related variations in MDF and MIF across the tree ring records and physiological
138 processes that may separate pools of Hg in the transport mechanism from atmosphere to foliage to
139 phloem to tree-ring/bole wood. Additionally, we aim to investigate if deposition and sorption of Hg
140 to tree bark is the dominant mechanism for bark Hg (isotopically distinct from bole wood).

141 **2. Methods**

142 **2.1. Study site**

143 The study area is in the High Black Forest (≈ 850 m a.s.l.) in Baden-Württemberg, Germany. Trees
144 were sampled within a 1 km radius of a former cyanisation facility that treated timber with $\approx 0.66\%$
145 HgCl_2 solution for preservation with substantial losses of this contaminated solution to soils,
146 groundwater, and stream water (Eisele, 2004, Richard et al., 2016; McLagan et al., 2022). Although
147 the trees were sampled within a 1 km radius of the contaminated site, all trees were outside, and
148 upslope of the area directly affected by Hg contamination to soils and groundwater. The location of
149 the sampled trees, former industrial buildings, wood drying areas, and passive sampling locations are
150 shown in Fig. 1. The history of the industrial activities at the site can be divided into three distinct
151 periods:



- 152 1. *Primary (first) industrial period (1stIP; 1892-1961)*: Reports on this contaminated site
153 describe the operation of the kyanisation facilities (wood treatment with 0.66 % HgCl₂) from
154 1892 until site owners went bankrupt in 1961 (Weis, 2020; Eisele, 2004; Schrenk and Hiester,
155 2007).
- 156 2. *Secondary industrial period (2ndIP; 1962-1992)*: The site was acquired by another company
157 and wood use and timber production as well as storage of timber treated with HgCl₂ is reported
158 to have continued at the site until 1992 (Eisele, 2004; Schrenk and Hiester, 2007).
- 159 3. *Background period (BGP; 1992-present)*: The site lay fallow between 1992 and 2002 before
160 site remediation (2002—2004) and conversion of the area to a commercial space (Eisele,
161 2004; Schrenk and Hiester, 2007).

162 These three periods will be referred to throughout the study under the descriptors of *1stIP*, *2ndIP*,
163 and *BGP*, respectively.

164 **2.2. Sampling and sample preparation**

165 Bole wood (tree ring) samples were collected via two methods. The first was using a 450 mm long,
166 5.15 mm diameter increment borer (Haglöf Sweden). The tree core was sampled at breast height
167 (\approx 1.2—1.5 m above ground). Whole tree core samples were placed in lab grade sampling straws and
168 double zip-seal bags for transport back to the lab. Spruce 1—3, spruce BG, and larch 1—3 were all
169 sampled by this method. Samples were counted for the visibly defined rings and cut with a disposable
170 scalpel.

171 The second method involved the collection of freshly cut (collected on day of tree felling) tree slices
172 or “cookies” (see TOC art; Section S1) from \approx 0.5 m above the ground. A \approx 50 mm slice was cut from
173 the middle of each tree cookie with a large table saw. Tree ring samples were cut from this slice with
174 a plain edge chisel. All exposed sides we cut away and discarded. Spruce ISO4—6 were sampled by
175 this method.

176 The number of tree rings (temporal resolution) in any given sample was typically 5 years but varied
177 somewhat with higher resolution in samples from some trees during *1stIP* and *2ndIP*, and lower in
178 some samples from spruce ISO trees that required higher THg concentrations per sample for Hg stable
179 isotope analyses. Samples were counted for rings, cut with a lab scalpel, weighed into nickel boats
180 and then combusted at 750 °C for 300 seconds. Care was taken to remove bark and phloem from
181 wood, but there may have been instances where some phloem remained attached to the newest tree
182 ring sample. Bark was sampled from spruce ISO4—6. Bark from spruce ISO4 and Spruce ISO5 were
183 divided into inner and outer bark (estimated as the middle of the bark) using a disposable scalpel.



184 After sample preparation samples were frozen (-20 °C), then freeze dried (-80 °C and 7 pa), and
185 subsequently stored at room temperature until analysis. Cleaning methods for equipment and surfaces
186 is detailed in Section S1. As these samples are from living (or freshly cut) trees no cross dating
187 methods were necessary; ring counting represents the most accurate method of dating. Sapwood was
188 visually identified by colour changes (Bertaud and Holmbom, 2004). However, any uncertainty
189 associated with identification of the exact number of sapwood rings is of little consequence to the
190 study as the greatest THg enrichment in sapwood was in the youngest tree rings, which, we can state
191 with certainty, were sapwood.

192 **2.3. Total Hg analyses**

193 THg concentration of samples collected with the increment borer were made using a thermal
194 desorption, amalgamation and atomic adsorption spectrometry (DMA80, Milestone Instruments).
195 Samples were counted for rings, cut with a lab scalpel (see borer cleaning methods), weighed into
196 nickel boats and then combusted at 750 °C for 300 seconds. Reference materials, Apple leaves (SRM
197 1515, NIST) and China Soil (NCS-DC73030; China National Analysis Centre for Iron and Steel),
198 were measured throughout the analyses and the recoveries were $103 \pm 3 \%$ ($n = 30$) and $99 \pm 5 \%$ (n
199 = 11), respectively. Details of the GEM passive air sampler methods and data can be found in Section
200 S2. THg concentration for the ISO trees were calculated from the analysis of traps after the pre-
201 concentration for isotope analysis (DMA-80L). All samples were considered on a dry-weight basis
202 (after freeze-drying) to remove any potential bias associated with moisture loss during transport and
203 storage before freezing.

204 **2.4. Hg stable isotope analyses**

205 Hg stable isotope analyses were performed on tree slice samples from trees: spruce ISO4—6. No
206 larch trees could be analysed for Hg stable isotopes as no larch tree slices could be collected. The low
207 THg concentration in many sections of the wood is a challenge for Hg stable isotope analyses. Low
208 concentration samples required pre-concentration and trapping by combusting samples in a DMA80
209 and then purging the released Hg from multiple boats of the same sample into 5 mL traps consisting
210 of 40 % (v/v) inverse aqua regia that replaced HCl with BrCl. Further method details (see also
211 McLagan et al. (2022)) and quality control/assurance of these analyses are provided in Section S4.
212 Traps with insufficient concentrations for isotope analysis were pool using the purge and trap method
213 detailed in Section S5. Hg stable isotope measurements were made using a Nu Plasma II (Nu
214 Instruments) inductively coupled plasma mass spectrometer (MC-ICP-MS) connected to an
215 HGX-200 cold vapour generator for Hg introduction (Teledyne Cetac) and a desolvating nebulizer



216 for external mass bias correction by Tl doping using NIST-997 (Aridus 2, Teledyne Cetac) following
217 a method previously established in our laboratory (see McLagan et al. (2022) and Wiederhold et al.
218 (2010) for method details). All samples and standards were diluted to match concentrations within
219 each session and samples were measured using standard bracketing with NIST-3133. Analytical
220 precision (2SD) and accuracy (using repeated measurements of “in-house” *ETH Fluka* standard and
221 NIST-3133 standards) for these analyses are reported in Section S6 along with full Hg stable isotope
222 datasets. Isotope ratios are reported as the deviation from the isotopic composition of the NIST-3133
223 standard using delta notation and expressed in per mil (‰) (details in Section S4).

224 **3. Results and Discussion**

225 **3.1. Elevated tree ring total Hg concentrations during industrial activity**

226 Elevated THg concentrations were observed in both Norway spruce (*P. abies*) and European larch
227 (*L. decidua*) tree rings dated before the mid-1990s compared to tree rings from the background
228 Norway spruce (spruce BG), which was situated ≈ 5.5 km west (upwind based on dominant westerly
229 winds in the area) of the former industrial facility (Fig. 2; THg data in Section S4). These species
230 were chosen due to suggested suitability for Hg archiving in previous studies (Hojdová et al., 2011;
231 Nováková et al., 2021) and there was a distinct pattern in tree ring THg concentrations in across all
232 sampled trees near the legacy contaminated site regardless of species. This resulted in four distinct
233 periods: (i) slightly elevated THg concentration in sapwood (hydroactive xylem) rings (0–5, 0–10,
234 or 0–15 year tree rings; see Section 3.3.2 for discussion), (ii) low THg concentration in rings from
235 the *BGP* not influenced by any known industrial activity (1992–sapwood), (iii) increasing THg
236 concentrations in rings from what we term the $2^{nd}IP$ (1962–1992), and (iv) very elevated THg
237 concentrations during the active kyanising or $1^{st}IP$ (before 1962) (Fig. 2). Not all sampled trees were
238 of sufficient age to cover all of these periods (no larch trees reached the $1^{st}IP$, but all trees that were
239 old enough did follow this trend albeit with some distinct inter-tree differences in THg concentrations
240 (Fig. 2).

241 The THg concentrations ranged from ≈ 1 – $10 \mu\text{g}\cdot\text{kg}^{-1}$ from tree rings in the *BGP* up to $521 \mu\text{g}\cdot\text{kg}^{-1}$
242 in a sample dated from 1951–1953 during the $1^{st}IP$ in spruce 1, which is ≈ 400 – 500 m northeast of
243 the former kyanisation building and wood drying areas. Additionally, THg concentrations of up to
244 $211 \mu\text{g}\cdot\text{kg}^{-1}$ were measured in a sample dated 1974–1976 ($2^{nd}IP$) in spruce 2, which was the closest
245 tree sampled to the former facility (≈ 200 – 300 m south). However, this tree was planted after the
246 $1^{st}IP$. Distance of the tree from the industrial source was a definite factor in the between tree
247 variability in THg concentrations, which has also been documented by Navrátil et al. (2017) and



248 Nováková et al. (2022). These THg concentrations are comparable to other studies with the high THg
249 concentrations measured in tree rings such as Becnel et al. (2004) (Loblolly Pine and Red Maple;
250 THg concentrations up to $644 \mu\text{g}\cdot\text{kg}^{-1}$), Abreu et al. (2008) (Black Poplar; THg concentrations up to
251 $280 \mu\text{g}\cdot\text{kg}^{-1}$), and Nováková et al. (2022) (European Larch; THg concentrations up to $249 \mu\text{g}\cdot\text{kg}^{-1}$).
252 However, the THg concentrations in our study are lower than the very high concentrations measured
253 by Wang et al. (2021) (Masson Pine; THg concentrations up to $2140 \mu\text{g}\cdot\text{kg}^{-1}$), which is likely
254 associated with the source being a former Hg mine known to have emitted large quantities of
255 elemental Hg (Hg(0)) to the atmosphere.

256 The THg concentrations in the tree rings generally provide a good representation of the industrial
257 history of the site based on the applied ≈ 5 -year sampling resolution. While the end of the $2^{\text{nd}}IP$ falls
258 in the middle of the 25—30 year tree ring samples, there is an increase in THg concentrations in all
259 trees in samples 30—35 year and greater (before 1990). This is most apparent in the spruce 1 and
260 spruce 2, which are the two sampled spruce trees closest to the former kyanisation building and wood
261 drying sites. The average THg concentration for spruce 1 and spruce 2 was significantly higher ($p =$
262 0.031 and $p < 0.001$, respectively) during the $2^{\text{nd}}IP$ (1962—1990; Spruce 1: $23.1 \pm 12.8 \mu\text{g}\cdot\text{kg}^{-1}$; and
263 spruce 2: $134 \pm 56 \mu\text{g}\cdot\text{kg}^{-1}$) than during the BGP (1990—sapwood; spruce 1: $10.8 \pm 2.6 \mu\text{g}\cdot\text{kg}^{-1}$; and
264 spruce 2: $9.46 \pm 3.65 \mu\text{g}\cdot\text{kg}^{-1}$). There was a sharp increase in THg concentration in the closest larch
265 tree to the site (larch 1) at this time, but the tree only dated to 1978, which is less than halfway through
266 the $2^{\text{nd}}IP$. Spruce 1 was also indicative of significantly higher ($p = 0.007$) THg concentrations during
267 the $1^{\text{st}}IP$ ($150 \pm 141 \mu\text{g}\cdot\text{kg}^{-1}$) compared to the elevated THg concentrations of the $2^{\text{nd}}IP$. These agrees
268 with other studies that have demonstrated good correlations between industrial activity and tree ring
269 Hg (Clackett et al., 2018; Navrátil et al., 2017; 2018; Nováková et al. 2022). Nonetheless, several
270 studies have suggested that Hg can translocate across tree rings, which results in temporal differences
271 between tree ring Hg and reported industrial activities/inventories (Nováková et al., 2021; Wang et
272 al., 2021). This should continue to be monitored closely in future studies, particularly considering the
273 sapwood enrichment discussed in Section 3.3.2.

274 Although the exact location of the three Spruce ISO trees (tree slices collected for Hg stable isotope
275 analysis) is unknown, they were from a deforested stand of spruce between 200—500 m further from
276 the wood drying site than spruce 1 on an easterly facing slope (away from the site). Consequently,
277 the mean THg concentrations in the spruce ISO4—6 were generally lower than in spruce 1.
278 Nonetheless, the same trends were observable: mean THg concentrations during the active industrial
279 period (before 1962, THg: $44.2 \pm 15.5 \mu\text{g}\cdot\text{kg}^{-1}$) were significantly greater ($p = 0.006$) than during the
280 $2^{\text{nd}}IP$ (1962—1990, THg: $26.7 \pm 15.7 \mu\text{g}\cdot\text{kg}^{-1}$), which were significantly greater ($p = 0.001$) than



281 rings from 1990—sapwood (THg: $6.5 \pm 4.6 \mu\text{g}\cdot\text{kg}^{-1}$) based on combined data from all three spruce
282 ISO trees.

283 **3.2. Isotopically fractionated Hg in tree rings associated with industrial emissions**

284 **3.2.1. Mass dependant fractionation (MDF)**

285 The THg concentration data from tree rings suggest substantial emissions of Hg to the atmosphere
286 during the industrial period. However, the original Hg contamination at these sites was the treatment
287 of timber with HgCl₂ solution, a species that has a high solubility and low volatility compared to
288 Hg(0) (Henry's Law constant: Hg(0): $1.4 \times 10^{-3} \text{ mol}\cdot\text{m}^{-3}\cdot\text{Pa}^{-1}$; HgCl₂: $2.7 \times 10^4 \text{ mol}\cdot\text{m}^{-3}\cdot\text{Pa}^{-1}$; Schroeder
289 and Munthe, 1998). Thus, the majority of any Hg releases to the atmosphere must have occurred via
290 reduction of Hg(II) to Hg(0) and subsequent volatilisation as GEM. Kinetic processes such as
291 reduction and evaporation result in the product (Hg released to the atmosphere in this case) becoming
292 enriched in lighter isotopes (more negative $\delta^{202}\text{Hg}$; Bergquist and Blum, 2007; 2009). Like the THg
293 concentrations, MDF values reflect a chronological trend: $\delta^{202}\text{Hg}$ values from the *1stIP* ($\delta^{202}\text{Hg}$: -4.32
294 $\pm 0.15 \text{ ‰}$, 1SD) were significantly more negative ($p = 0.007$) than during the *2ndIP* ($\delta^{202}\text{Hg}$: $-4.02 \pm$
295 0.31 ‰ ; 1SD), which in turn were significantly more negative ($p < 0.001$) than rings from the *BGP*
296 ($\delta^{202}\text{Hg}$: $-2.76 \pm 0.76 \text{ ‰}$, 1SD; sapwood 0–5 year samples not included, see Section 3.3.2) based on
297 combined data from all three spruce ISO trees (Fig. 3A). Wang et al. (2021) observed similar,
298 although weaker, trends in Masson pines near Hg contaminated sites in China (range: -5.06 ‰ to
299 -2.53 ‰ ; median: -3.74 ‰). MDF ($\delta^{202}\text{Hg}$) has also been examined in oak ($-1.82 \pm 0.09 \text{ ‰}$) and
300 pitch pine ($-2.98 \pm 0.76 \text{ ‰}$; North America; Scanlon et al., 2020), conifers ($-2.76 \pm 0.46 \text{ ‰}$; China;
301 Liu et al., 2021), evergreen trees ($-3.15 \pm 0.22 \text{ ‰}$; China; Wang et al., 2020), and harvested one-year
302 old Norway spruce saplings ($-2.71 \pm 0.27 \text{ ‰}$; Germany; Yamakawa et al., 2021). $\delta^{202}\text{Hg}$ values in
303 these studies were more similar to samples from the *BGP* in our study, which likely relates to their
304 low bole wood THg concentrations associated with the remoteness of their study sites from
305 contamination sources (Scanlon et al., 2020; Wang et al., 2020; Liu et al., 2021; Yamakawa et al.,
306 2021).

307 McLagan et al. (2022) highlight the difficulties in characterising a specific source signature of Hg
308 stocks used in industrial activities due to the variability in stock $\delta^{202}\text{Hg}$ values, potential change in
309 Hg supplies during the facility's lifetime, and the possibility that the industrial use of Hg resulted in
310 the Hg emitted to different environmental media being fractionated from the original Hg stock. The
311 highly negative $\delta^{202}\text{Hg}$ values during both the *1stIP* and *2ndIP* support the hypothesis that there was
312 significant loss of Hg to the atmosphere during the industrial activities, which would result in the



313 residual HgCl_2 in solution (major source of soil-groundwater contamination) being isotopically
314 heavier than the original Hg stocks used at the site. Indeed, solid phase materials (listed as “SCA1”
315 and “TSA” in McLagan et al., 2022) beneath the former kyanisation plant with THg concentrations
316 $>50 \mu\text{g}\cdot\text{kg}^{-1}$ had mean $\delta^{202}\text{Hg}$ values of $0.06 \pm 0.23 \text{ ‰}$ (McLagan et al., 2022). This is at the positive
317 end of the range of $\delta^{202}\text{Hg}$ values reported for cinnabar ores and commercial liquid Hg^0 stocks (Sun
318 et al., 2016; Grigg et al., 2018).

319 $\delta^{202}\text{Hg}$ for GEM in background air is typically in the range of ≈ -0.2 to 1.5 ‰ (Szponar et al., 2020
320 and references therein). Foliar uptake of GEM is reported to cause substantial MDF of between -2.3
321 and -2.9 ‰ (Demers et al., 2013; Enrico et al., 2016; Wang et al., 2021). If we subtract the middle of
322 the estimated range of MDF caused by foliar uptake ($\delta^{202}\text{Hg}$: $-2.6 \pm 0.3 \text{ ‰}$) from the mean $\delta^{202}\text{Hg}$
323 values measured in tree rings during *1stIP* and *2ndIP* we get $\delta^{202}\text{Hg}$ estimates of $-1.7 \pm 0.2 \text{ ‰}$ and -1.4
324 $\pm 0.2 \text{ ‰}$ (propagated uncertainty), respectively, for GEM during these periods at the approximate
325 location of the southeast facing forest stand where the spruce ISO trees were sampled (see also Fig.
326 4). This agrees with other studies that suggest industrial sources of Hg are enriched in lighter isotopes
327 compared to background air (Jiskra et al., 2019; Szponar et al., 2020, and references therein). These
328 estimates assume Hg in tree rings is derived from foliar uptake of GEM from the atmosphere, which
329 is suggested to be the dominant uptake pathway of Hg in trees (e.g., Beauford et al., 1977; Graydon
330 et al. 2009; Cozzolino et al., 2016), and no further MDF during downward transport of Hg within the
331 trees (as observed by Liu et al., 2021).

332 Applying the same correction to the $\delta^{202}\text{Hg}$ in tree rings from the *BGP* we get a $\delta^{202}\text{Hg}$ estimate of
333 $-0.2 \pm 0.3 \text{ ‰}$ for GEM during this time (see also Fig. 4). This is right on the lower end of the reported
334 range for $\delta^{202}\text{Hg}$ of typical background GEM and suggests there may still be some minor inputs of
335 Hg from the still contaminated soils (McLagan et al., 2022) to the trees during the *BGP*. GEM
336 concentrations were measured with PASs over the areas of the former kyanisation building and wood
337 drying areas ($2.9 \pm 0.6 \text{ ng}\cdot\text{m}^{-3}$) and concentrations were approximately double typical European
338 background concentrations ($\approx 1.5\text{—}2.0 \text{ ng}\cdot\text{m}^{-3}$) (Sprovieri et al., 2016). Other studies that have
339 observed more elevated GEM concentrations with co-located GEM PAS deployments: up to three
340 orders of magnitude higher concentrations at a former Hg mine (McLagan et al., 2018) and 3–4x
341 higher at a Hg contaminated waste site (McLagan et al., 2021b). Therefore, we can assume the slightly
342 elevated GEM concentrations detected at the site in 2018 are associated with low-level GEM emission
343 from the site. These minor emissions likely cause a small negative shift in $\delta^{202}\text{Hg}$ values of the tree
344 rings from what might be expected of “true” background values. To our knowledge this is the first
345 study to address elevated GEM concentrations from a former Hg kyanisation facility.



3.2.2. Mass independent fractionation (MIF)

We also observed small variability in odd isotope-MIF in the spruce ISO tree rings (Fig. 3B). The mean $\Delta^{199}\text{Hg}$ for the $1^{st}IP$ ($\Delta^{199}\text{Hg}$: 0.00 ± 0.03 ‰, 1SD) was significantly greater ($p < 0.001$) than for the $2^{nd}IP$ ($\Delta^{199}\text{Hg}$: -0.06 ± 0.04 ‰, 1SD), which in turn was significantly greater ($p < 0.001$) than the BGP ($\Delta^{199}\text{Hg}$: -0.13 ± 0.03 ‰, 1SD). The $\Delta^{199}\text{Hg}$ of the $1^{st}IP$ is right at the mean values for cinnabar ores ($\Delta^{199}\text{Hg}$: 0.01 ± 0.10 ‰, 1SD) and liquid Hg(0) stocks ($\Delta^{199}\text{Hg}$: -0.01 ± 0.03 ‰, 1SD) (Sun et al., 2016; Grigg et al., 2018). Additionally, the mean $\Delta^{199}\text{Hg}$ values from the solid phase materials at this contaminated site were -0.01 ± 0.06 ‰ (McLagan et al., 2022). Hence, we suggest $\Delta^{199}\text{Hg}$ values in the tree rings during $1^{st}IP$ are conserved from the industrial activities.

Wang et al. (2021) made similar observations in Masson Pine tree rings near a former Hg mine in Guizhou Province of China: more positive $\Delta^{199}\text{Hg}$ values during periods of more intense industrial activity. The more negative $\Delta^{199}\text{Hg}$ values in tree rings from the BGP are similar to the more negative background GEM values (typical range: -0.4 to 0.0 ‰; Szponar et al., 2020 and references therein). Scanlon et al. (2020) measured low THg concentration ($<4.5 \mu\text{g}\cdot\text{kg}^{-1}$) in red oak, white oak, and pitch pine tree rings and negative $\Delta^{199}\text{Hg}$ values (-0.39 to -0.14 ‰) and also associated this with the characteristic GEM signature of background air. The difference in $\Delta^{199}\text{Hg}$ between the $1^{st}IP$, $2^{nd}IP$, and BGP is likely related to the atmospheric mixing of background GEM with industrially derived Hg. Foliar uptake has been reported to impart a small negative $\Delta^{199}\text{Hg}$ shift (≈ -0.1 to -0.2 ‰; Demers et al., 2013; Yuan et al., 2018). Yet, our data were more indicative of sources (industrial or background); thus, any negative $\Delta^{199}\text{Hg}$ shift may be small in Norway spruce and/or differences fall within the range of variability of the sources.

Information on the specific processes driving odd-MIF (nuclear volume effect (NVE) vs magnetic isotope effect (MIE)) in the measured Hg can be derived from the ratio of $\Delta^{199}\text{Hg}$ to $\Delta^{201}\text{Hg}$ (Bergquist and Blum, 2007; Blum et al., 2014). We derived a slope of 1.25 ± 0.13 (1SE) for bole wood using York orthogonal regression (Fig. S8.1; York et al., 2004), which is higher than other studies (1.04 in Wang et al., 2021; and 1.05 in Scanlon et al., 2020 and Liu et al., 2021), but still lies in the range of the expected slope (1.0—1.3) for MIE related photochemical reduction of Hg(II) to Hg(0) (Bergquist and Blum, 2007; Zheng et al., 2009). The observed MIF data suggest MIE related photochemical reduction and subsequent Hg(0) evasion is likely the dominant pathway of Hg(0) to the atmosphere. However, we caution against the over interpretation of these data as there was a large difference in the slope using a different orthogonal regression method (Fig. S8.1; Deming 1943). This difference in methods can largely be explained by the limited extent of odd-MIF observed in the tree ring data.



378 Both, $\Delta^{200}\text{Hg}$ and $\Delta^{204}\text{Hg}$ values show there was no significant even isotope-MIF in the bole wood
379 samples (Section S8). $\Delta^{200}\text{Hg}$ anomalies have been reported for Hg in precipitation samples and
380 related to upper atmosphere oxidation of Hg(0) (Gratz et al., 2010; Chen et al., 2012). Thus, the near
381 zero even-MIF supports the hypothesis that the Hg in tree rings relates to foliar uptake of atmospheric
382 GEM (unaffected by even-MIF) rather than root uptake of Hg deposited to soils via wet deposition
383 of Hg(II).

384 **3.3. Physiological and species related factors impacting within tree Hg cycling**

385 **3.3.1. THg concentration and stable Hg isotopes in bark**

386 THg concentrations in the bark of three spruce ISO trees ($137 \pm 105 \mu\text{g}\cdot\text{kg}^{-1}$) were significantly
387 higher than THg in bole wood of *BGP* ($p = 0.014$), 2^{nd}IP ($p = 0.025$), and 1^{st}IP ($p = 0.042$).
388 Furthermore, the bark was divided into inner (younger) and outer (older) bark of spruce ISO4 and
389 ISO5 trees and the outer bark was 2.0 and 2.7x higher in THg concentrations, respectively. This is
390 similar to the observations made by Chiarantini et al. (2016) for black pine and could be related to
391 longer and more exposure of the outer bark to elevated atmospheric Hg concentrations leading to
392 more Hg deposited to these layers. Nonetheless, the older, outer bark would have been closer to the
393 phloem (inner most bark layer; likely pathway for downward transport of Hg in trees) during the 1^{st}IP
394 and 2^{nd}IP when we expect GEM concentrations were much higher than they are presently. Moreover,
395 the inner bark concentrations (spruce ISO4: $57.7 \mu\text{g}\cdot\text{kg}^{-1}$; spruce ISO5: $163.1 \mu\text{g}\cdot\text{kg}^{-1}$) were still
396 elevated with reference to the *BGP* in particular. Arnold et al. (2018) and Peckham et al. (2019a)
397 suggest that translocation of Hg from the phloem into the inactive inner bark layers may be an
398 important source of Hg stored within bark, which they further suggest supports findings by
399 Chiarantini et al. (2016) that inner bark layers have a higher proportion of “organic Hg” than the outer
400 layers in black pine.

401 If the predominant source of Hg in bark was via deposition of either GEM or GOM/PBM then we
402 would expect to observe more positive $\delta^{202}\text{Hg}$ values in the bark samples as this pathway is unaffected
403 by the large negative MDF ($\approx -2.6\%$) associated with stomatal uptake. However, the $\delta^{202}\text{Hg}$ values
404 for the bark samples were all highly negative ($\delta^{202}\text{Hg}$: $-3.90 \pm 0.30\%$, 1SD) and similar to the highly
405 negative values in tree ring samples from the 1^{st}IP and 2^{nd}IP . Furthermore, GOM/PBM is reported to
406 have more positive $\Delta^{199}\text{Hg}$ values than GEM (Szponar et al., 2020), but the bark samples ($\Delta^{199}\text{Hg}$:
407 $-0.14 \pm 0.06\%$, 1SD) were similar if not slightly more negative than the bole wood from these
408 industrial periods (Fig. 4). There was very little difference in $\delta^{202}\text{Hg}$ or $\Delta^{199}\text{Hg}$ between the inner and
409 outer bark of either spruce ISO4 or ISO5 tree (Table S4.1). In summary, our Hg stable isotope data



410 suggests the stomatal uptake, internal transport, and translocation from phloem to inner bark is likely
411 the dominant uptake pathway for Hg stored in bark. Liu et al. (2021) posited the same foliage
412 assimilation pathway for bark Hg uptake based on similar $\delta^{202}\text{Hg}$ and $\Delta^{199}\text{Hg}$ values in both their bark
413 and bole wood samples from subtropical evergreen species at a background site. Considering *rays*
414 that connect xylem and phloem reach as far as the inner bark (Nagy et al., 2014; Pfautsch et al., 2015),
415 this mechanism of bark Hg enrichment is a distinct possibility. More data across a range of species,
416 particularly using Hg stable isotopes, would be beneficial to determine the robustness of this
417 conclusion.

418 3.3.2. Sapwood (hydroactive xylem) rings enriched in Hg

419 THg concentrations were elevated in sapwood tree ring samples of all trees from both species,
420 including spruce BG, compared to tree rings from the *BGP*. The 0—5 year samples were elevated in
421 all trees and the 5—10 and 10—15 year samples were also higher in THg concentrations in some
422 trees (Fig. 2). Although part of the phloem (first layer of bark) may have been included in some 0—
423 5 year samples and contributed to enrichment of these samples, elevated THg concentrations in
424 certain 5—10 and 10—15 year samples indicate this is not the sole determinant. Sapwood enrichment
425 has also been observed in both Norway spruce (Hojdová et al., 2011) and European larch (Navrátil et
426 al., 2018; Nováková et al., 2021; 2022) and various species of oak and pine (Wright et al., 2014;
427 Navrátil et al., 2017; Scanlon et al., 2020; Wang et al., 2021). Our study represents perhaps the most
428 pronounced and consistent (across all trees) example of this sapwood enrichment. Nováková et al.
429 (2021) suggest the tree coring sampling method could be a potential source of this enrichment.
430 However, we observe this in the spruce ISO trees that were sampled by breaking up tree “cookies”
431 rather than coring, which would rule out this possibility.

432 We examine three alternate scenarios to explain this. The first is that GEM concentrations in the
433 area have been elevated during the last decade compared to the *BGP*. While the PAS measured GEM
434 concentrations were slightly elevated ($\approx 2\times$ European background concentrations) likely associated
435 with minor on-going releases from contaminated topsoils, there is no evidence to suggest why GEM
436 concentrations in the most recent 5—10 years would be higher than the earlier *BGP*. Additionally,
437 the spruce BG tree also had elevated THg concentrations in all samples under 15 years, which had
438 little-to-no impact in tree ring Hg by the industrial facility during *1stIP* or *2ndIP*. The European
439 Monitoring and Evaluation Programme (EMEP) has a long-term monitoring station $\approx 22\text{km}$ to the
440 west of the former industrial site ($\approx 16.5\text{ km}$ west of spruce BG) and reports a mean total gaseous Hg
441 (predominantly GEM) concentration of $1.49\text{ ng}\cdot\text{m}^{-3}$ over the last decade (EMEP, 2022), which is a



442 typical background concentration for Europe (Sprovieri et al., 2016). Hence, recently elevated GEM
443 concentrations cannot explain the elevated sapwood THg concentrations.

444 The second would relate to uptake of Hg from tree roots. The conductive or actively transporting
445 component of xylem (hydroactive xylem) exists within the sapwood of trees. Its primary role is the
446 upward transport of water and nutrients from tree roots to the aerial components and particularly
447 leaves/needles. We have already discussed how this pathway has been shown to be a minor
448 mechanism of Hg uptake in many studies (e.g., Beauford et al., 1977; Graydon et al. 2009; Cozzolino
449 et al., 2016). Also, the sampled trees are outside the area in which surface contamination from the
450 industrial activity occurred (particularly spruce BG); any soil contamination must have come from
451 atmospheric Hg emissions and subsequent deposition, of which stomatal uptake of GEM is the
452 dominant conduit in forest ecosystems (Obrist et al., 2017; 2018; Jiskra et al., 2018). We consider
453 this mechanism highly unlikely to be driving sapwood enrichment.

454 The third scenario relates to tree physiology. Hg is transported downwards in trees via the phloem
455 and has been reported to translocate from phloem to xylem (sapwood) throughout this process
456 (Arnold et al., 2018; Yanai et al., 2020; Nováková et al., 2021). As sapwood ages it undergoes a
457 physiological transition to heartwood, which is drier, contains predominantly dead cells, and is used
458 for structure rather than transport (Bertaud and Holmbom, 2004; Metsä-Kortelainen et al., 2006). Hg
459 that remains in the tree rings after the transition to heartwood likely binds to components that endure
460 this change, but there is a caveat in our knowledge of this process (Yanai et al., 2020; Nováková et
461 al., 2021). Since we use dry weight THg concentrations, if all the Hg translocated from phloem to
462 xylem was conserved in the wood during the transition from sapwood to heartwood, then we would
463 not expect to see any sapwood enrichment. Thus, we deem it likely that some fraction of Hg is retained
464 in the xylem solution or structures/chemicals enhanced in sapwood (compared to heartwood) of these
465 species. Although we only have two samples from the 0–5 year tree rings analysed for stable
466 isotopes, the $\delta^{202}\text{Hg}$ data from spruce ISO5 and ISO 6 are shifted negative (-0.41 and -0.33 ‰,
467 respectively) in these samples compared to the adjacent composite sample of tree rings in each
468 respective tree (Fig. 3A; Section S6). Hence, the process controlling retention of this Hg in sapwood
469 would seem to favour lighter isotopes, implying there could be either preferential retention of specific
470 Hg-compounds or a change in binding form during the retention process.

471 Any upwards transport of xylem solution Hg may contribute to the slightly elevated THg
472 concentrations that Yanai et al. (2020) observed in tree rings at higher elevations above the ground.
473 Sapwood is also a storage reserve for energy (starch) and water (Taylor et al., 2002); therefore, some



474 of the Hg in xylem solution may be stored long-term in the hydroactive xylem without being
475 transferred as the sapwood rings transition to heartwood. While long-term storage of some Hg in
476 sapwood could be a factor driving temporal differences between tree ring THg concentrations and
477 reported industrial activity in the literature (Arnold et al., 2018; Wang et al., 2021), our data do not
478 reflect such Hg translocation. Ultimately, further research will be needed, particularly using Hg stable
479 isotopes, to further explore this hypothesis and the physiological mechanisms behind this enrichment.

480 **3.3.3. The impact of species on uptake and storage of Hg in tree rings**

481 There is extensive discussion in the literature on species specific differences in THg concentrations
482 of tree rings, particularly as they relate to foliar uptake rates (Wohlgemuth et al., 2020) and inter-ring
483 translocation (Arnold et al., 2018; O'Connor et al., 2019). Inter-ring translocation has led some
484 studies to question the overall effectiveness using tree rings as an archive for atmospheric GEM, but
485 many of these studies have utilised oak (Scanlon et al., 2020), some pine species (Wang et al., 2021;
486 Nováková et al., 2021), and Populus (Arnold et al., 2018). Certain physiological characteristics of
487 these species (i.e., more radially conductive xylem) that enhance this translocation may limit their
488 applicability to tree ring atmospheric archiving (Arnold et al., 2018; Nováková et al., 2021; Gustine
489 et al., 2022). Several studies have observed strong correlations between THg concentrations in spruce
490 (Hojdová et al., 2011) and larch (Navrátil et al., 2018; Nováková et al., 2021) tree rings and reported
491 industrial activities and suggest these to be appropriate species for archiving atmospheric GEM
492 concentrations.

493 Despite the quite apparent physiological differences between European larch (deciduous conifer)
494 and Norway spruce (evergreen conifer), trends in THg concentrations varied little between the
495 sampled trees of either species. Sapwood was enriched, *BGP* THg was low, and concentrations
496 increased into the *2ndIP* at the same time (early 1990s) in both larch and spruce trees (all sampled
497 larch were planted after the *1stIP*) (Fig. 2). Additionally, the good correlation between changes in
498 THg concentrations and the timelines of the *1stIP*, *2ndIP*, and *BGP* suggest the process driving
499 sapwood Hg enrichment results in limited inter-ring Hg translocation in Norway spruce and European
500 larch; the fraction of Hg transferred to heartwood must be relatively consistent under this scenario.
501 Thus, our data too suggest Norway spruce and European larch are effective species for the chronicling
502 of historic GEM concentrations.

503 **3.3.4. Between and within tree variability in tree ring Hg**

504 Heterogeneity in the radial distribution of Hg has been observed in other studies and authors suggest
505 sampling of multiple trees in each stand and different radial sections of trees provides more



506 representative assessments (Wright et al., 2014; Peckham et al., 2019b). The sampling direction of
507 the bole or height of the sampling can cause differences within replicate samples from the same tree.
508 Factors affecting between tree variability include microtopography, tree age or species and related
509 specific physiological differences such as photosynthesis rate, stomatal conductance and transpiration
510 (Binda et al., 2021). No correlation between Hg concentration and tree core mass was reported by
511 Scanlon et al. (2020) and they concluded that differences in radial growth do not dilute or concentrate
512 Hg in tree rings. These authors therefore concluded that Hg concentrations are a suitable proxy to
513 evaluate trends of GEM. We detected some variability in THg concentrations between spruce ISO4,
514 ISO5, and ISO6 from the same stand of trees (Fig. 2) and in “replicated” tree rings from different
515 sides of the spruce ISO tree slices (mean relative difference: $78 \pm 35 \%$; mean absolute difference: 5
516 $\pm 5 \mu\text{g}\cdot\text{kg}^{-1}$; $n = 10$; Table S3.1). Yet, variability in the ratios of Hg stable isotopes within the bole
517 wood was low (mean absolute difference: $\delta^{202}\text{Hg}$: $0.11 \pm 0.08 \text{‰}$ 1SD; $\Delta^{199}\text{Hg}$: $0.08 \pm 0.02 \text{‰}$ 1SD;
518 $n = 4$; Table S4.2). This suggests factors influencing radial Hg heterogeneity cause little impact of
519 Hg stable isotopes. We considered the stable isotopes analyses based on combined data from all three
520 trees, but individual trees also followed these trends (Section S6).

521 **Data availability**

522 All data are available within the paper and supplementary information. If there are any additional
523 requests, please contact the authors.

524 **Supplementary information**

525 The Supporting Information is available free of charge at DOI: XXX.

526 **Author Contribution**

527 The project design and planning were made by DSM and LS, with inputs from TN. The manuscript
528 was written predominantly by DSM with inputs from LS. Figures were prepared by DSM and LS.
529 Supplemental information was prepared predominantly by LS with inputs from DSM. Tree core
530 sampling was performed by DSM and LS, HB collected tree slices/“cookies”. THg analyses were
531 performed by LS and DSM, passive samplers were analysed by DSM, pre-concentration and isotope
532 analysis was performed by LS. Lab space provided by HB and SMK. DSM, LS, HB, and TN
533 contributed to manuscript reviews. DSM and LS contributed equally to this work.

534 **Conflicts of Interest**

535 The authors declare no competing financial interest.



536 Acknowledgements

537 We would like to acknowledge Herwig Lenitz, Petra Schmidt, and Adelina Caelean for analytical
538 assistance and discussions with analysis, Sofie M. Reiter for the assistance with the pre-concentration
539 of the isotope samples, Jan Wiederhold for discussion on data, Jan Pietrucha for help assessing site
540 reports and assistance in analysis, Matthias Beyer for use of the increment borer. This research was
541 funded by the German Research Foundation (DFG) grant BI 734/17-1 and the Austrian Science Fund
542 (FWF) grant I-3489-N28.

543 References

544 Abreu, S. N., Soares, A. M. V. M., Nogueira, A. J. A., and Morgado, F.: Tree rings, *Populus nigra*
545 L.; as mercury data logger in aquatic environments: Case study of an historically contaminated
546 environment, *Bull. Environ. Contam. Toxicol.*, 80(3), 294-299. DOI: 10.1007/s00128-008-9366-0,
547 2008.

548 Arnold, J., Gustin, M. S., and Weisberg, P. J.: Evidence for nonstomatal uptake of Hg by aspen and
549 translocation of Hg from foliage to tree rings in Austrian pine, *Environ. Sci Technol.*, 52(3), 1174-
550 1182, DOI: 10.1021/acs.est.7b04468, 2018.

551 Beauford, W., Barber, J., and Barringer, A. R.: Uptake and distribution of mercury within higher
552 plants, *Physiol. Plant.*, 39(4), 261-265, DOI: 10.1111/j.1399-3054.1977.tb01880.x, 1977.

553 Becnel, J., Falgeust, C., Cavalier, T., Gauthreaux, K., Landry, F., Blanchard, M., Beck, M. J., and
554 Beck, J.N.: Correlation of mercury concentrations in tree core and lichen samples in southeastern
555 Louisiana, *Microchem. J.*, 78(2), 205-210, DOI: 10.1016/j.microc.2004.06.002, 2004.

556 Bergquist, B. A., and Blum, J. D.: Mass-dependent and-independent fractionation of Hg isotopes
557 by photoreduction in aquatic systems, *Sci.*, 318(5849), 417-420, DOI: 10.1126/science.1148050,
558 2007.

559 Bergquist, B. A., and Blum, J. D.: The odds and evens of mercury isotopes: applications of mass-
560 dependent and mass-independent isotope fractionation, *Elements*, 5(6), 353-357, DOI:
561 10.2113/gselements.5.6.353, 2009.

562 Bertaud, F., and Holmbom, B.: Chemical composition of earlywood and latewood in Norway spruce
563 heartwood, sapwood and transition zone wood, *Wood Sci. Technol.*, 38(4), 245-256, DOI:
564 10.1007/s00226-004-0241-9, 2004.

565 Binda, G., Di Lorio, A., and Monticelli, D.: The what, how, why, and when of dendrochemistry:



- 566 (paleo)environmental information from the chemical analysis of tree rings, *Sci. Tot. Environ.*, 758,
567 143672, DOI: 10.1016/j.scitotenv.2020.143672, 2021.
- 568 Bishop, K. H., Lee, Y. H., Munthe, J., and Dambrine, E.: Xylem sap as a pathway for total mercury
569 and methylmercury transport from soils to tree canopy in the boreal forest, *Biogeochem.*, 40(2), 101-
570 113, DOI: 10.1023/A:1005983932240, 1998.
- 571 Blum, J. D., Sherman, L. S., and Johnson, M. W.: Mercury isotopes in earth and environmental
572 sciences, *Annu. Rev. Earth Planet. Sci.*, 42, 249-269, DOI: 10.1146/annurev-earth-050212-124107,
573 2014.
- 574 Browne, C. L., and Fang, S. C.: Uptake of mercury vapor by wheat: an assimilation model, *Plant*
575 *Physiol.*, 61(3), 430-433, DOI: 10.1104/pp.61.3.430, 1978.
- 576 Chen, J., Hintelmann, H., Feng, X., and Dimock, B.: Unusual fractionation of both odd and even
577 mercury isotopes in precipitation from Peterborough, ON, Canada, *Geochim. Cosmochim. Acta*, 90,
578 33-46, DOI: 10.1016/j.gca.2012.05.005, 2012.
- 579 Chiarantini, L., Rimondi, V., Benvenuti, M., Beutel, M. W., Costagliola, P., Gonnelli, C., Lattanzi,
580 P., and Paolieri, M.: Black pine (*Pinus nigra*) barks as biomonitors of airborne mercury pollution, *Sci.*
581 *Total Environ.*, 569, 105-113, DOI: 10.1016/j.scitotenv.2016.06.029, 2016.
- 582 Chiarantini, L., Rimondi, V., Bardelli, F., Benvenuti, M., Cosio, C., Costagliola, P., Di Benedetto,
583 F., Lattanzi, P., and Sarret, G.: Mercury speciation in *Pinus nigra* barks from Monte Amiata (Italy):
584 An X-ray absorption spectroscopy study, *Environ. Pollut.*, 227, 83-88, DOI:
585 10.1016/j.envpol.2017.04.038, 2017.
- 586 Clackett, S. P., Porter, T. J., and Lehnher, I.: 400-year record of atmospheric mercury from tree-
587 rings in Northwestern Canada, *Environ. Sci. Technol.*, 52(17), 9625-9633, DOI:
588 10.1021/acs.est.8b01824, 2018.
- 589 Cozzolino, V., De Martino, A., Nebbioso, A., Di Meo, V., Salluzzo, A., and Piccolo, A.: Plant
590 tolerance to mercury in a contaminated soil is enhanced by the combined effects of humic matter
591 addition and inoculation with arbuscular mycorrhizal fungi, *Environ. Sci. Pollut. Res.*, 23(11), 11312-
592 11322, DOI: 10.1007/s11356-016-6337-6, 2016.
- 593 Cui, L., Feng, X., Lin, C. J., Wang, X., Meng, B., Wang, X., and Wang, H.: Accumulation and
594 translocation of ¹⁹⁸Hg in four crop species, *Environ. Toxicol. Chem.*, 33(2), 334-340, DOI:
595 10.1002/etc.2443, 2014.



- 596 Cutter, B. E., and Guyette, R. P.: Anatomical, chemical, and ecological factors affecting tree species
597 choice in dendrochemistry studies, *J. Environ. Qual.*, 22(3), 611-619, DOI:
598 10.2134/jeq1993.00472425002200030028x, 1993.
- 599 Dastoor, A., Angot, H., Bieser, J., Christensen, J., Douglas, T., Heimbürger-Boavida, L. E., Jiskra,
600 M., Mason, R., McLagan, D. S., Obrist, D., Outridge, P., Petrova, M., Ryjkov, A., St. Pierre, K.,
601 Schartup, A., Soerensen, A., Travnikov, O., Toyota, K., Wilson, S., and Zdanowicz, C.: Arctic
602 mercury cycling, *Nat. Rev. Earth Environ.*, 3, 270-286, DOI: 10.1038/s43017-022-00269-w, 2022.
- 603 Demers, J. D., Blum, J. D., and Zak, D. R.: Mercury isotopes in a forested ecosystem: Implications
604 for air-surface exchange dynamics and the global mercury cycle, *Global Biogeochem. Cy.*, 27(1),
605 222-238, DOI: 10.1002/gbc.20021, 2013.
- 606 Deming, W. E.: *Statistical adjustment of data*. Wiley, New Jersey, USA, 1943.
- 607 Dennis, K. K., Uppal, K., Liu, K. H., Ma, C., Liang, B., Go, Y. M., and Jones, D. P.: Phytochelatin
608 database: a resource for phytochelatin complexes of nutritional and environmental metals, Database,
609 2019, baz083, DOI: 10.1093/database/baz083, 2019.
- 610 Eisele, G.: Arbeitshilfe Absicherbarkeit von Risiken beim Flächenrecycling, Forschungsbericht
611 FZKA-BWPLUS, Landesanstalt für Umwelt Baden-Württemberg, Baden-Württemberg, Germany,
612 102. <https://pd.lubw.de/99447>, 2004.
- 613 EMEP: Co-operative Programme for Monitoring and Evaluation of the Long-Range Transmissions
614 of Air Pollutants in Europe, European Monitoring and Evaluation Programme (EMEP), Kjeller,
615 Norway. <https://projects.nilu.no/ccc/reports.html>, accessed: Feb 09, 2022, 2022.
- 616 Enrico, M., Roux, G. L., Maruszczak, N., Heimbürger, L. E., Claustres, A., Fu, X., Sun, R., and
617 Sonke, J. E.: Atmospheric mercury transfer to peat bogs dominated by gaseous elemental mercury
618 dry deposition, *Environ. Sci Technol.*, 50(5), 2405-2412, DOI: 10.1021/acs.est.5b06058, 2016.
- 619 Friedli, H. R., Arellano, A. F., Cinnirella, S., and Pirrone, N.: Initial estimates of mercury emissions
620 to the atmosphere from global biomass burning, *Environ. Sci Technol.*, 43(10), 3507-3513, DOI:
621 10.1021/es802703g, 2009.
- 622 Gratz, L. E., Keeler, G. J., Blum, J. D., and Sherman, L. S.: Isotopic composition and fractionation
623 of mercury in Great Lakes precipitation and ambient air, *Environ. Sci Technol.*, 44(20), 7764-7770,
624 DOI: 10.1021/es100383w, 2010.
- 625 Graydon, J. A., St. Louis, V. L., Hintelmann, H., Lindberg, S. E., Sandilands, K. A., Rudd, J. W.,



626 Kelly, C. A., Tate, M. T., Krabbenhoft, D. P., and Lehnher, I.: Investigation of uptake and retention
627 of atmospheric Hg (II) by boreal forest plants using stable Hg isotopes, *Environ. Sci Technol.*, 2009,
628 43(13), 4960-4966, DOI: 10.1021/es900357s, 2009.

629 Grigg, A. R., Kretzschmar, R., Gilli, R. S., and Wiederhold, J. G.: Mercury isotope signatures of
630 digests and sequential extracts from industrially contaminated soils and sediments. *Sci. Total*
631 *Environ.*, 2018, 636, 1344-1354, DOI: 10.1016/j.scitotenv.2018.04.261, 2018.

632 Gustin, M. S., Ingle, B., and Dunham-Cheatham, S. M.: Further investigations into the use of tree
633 rings as archives of atmospheric mercury concentrations, *Biogeochem.*, 158, 167-180, DOI:
634 10.1007/s10533-022-00892-1, 2022.

635 Hojdová, M., Navrátil, T., Rohovec, J., Žák, K., Vaněk, A., Chrástný, V., Bače, R., and Svoboda,
636 M.: Changes in mercury deposition in a mining and smelting region as recorded in tree rings, *Water*
637 *Air Soil Pollut.*, 216(1), 73-82, DOI: 10.1007/s11270-010-0515-9, 2011.

638 Jiskra, M., Wiederhold, J. G., Skjellberg, U., Kronberg, R. M., Hajdas, I., and Kretzschmar, R.:
639 Mercury deposition and re-emission pathways in boreal forest soils investigated with Hg isotope
640 signatures, *Environ. Sci Technol.*, 49(12), 7188-7196, DOI: 10.1021/acs.est.5b00742, 2015.

641 Jiskra, M., Sonke, J. E., Obrist, D., Bieser, J., Ebinghaus, R., Myhre, C. L., Pfaffhuber, K. A.,
642 Wängberg, I., Kyllönen, K., Worthy, D., and Martin, L. G.: A vegetation control on seasonal
643 variations in global atmospheric mercury concentrations, *Nature Geosci.*, 11(4), 244-250, DOI:
644 10.1038/s41561-018-0078-8, 2018.

645 Jiskra, M., Maruszczak, N., Leung, K. H., Hawkins, L., Prestbo, E., and Sonke, J. E.: Automated
646 stable isotope sampling of gaseous elemental mercury (ISO-GEM): Insights into GEM emissions
647 from building surfaces, *Environ. Sci Technol.*, 53(8), 4346-4354, DOI: 10.1021/acs.est.8b06381,
648 2019.

649 Kahle, H.: Response of roots of trees to heavy metals, *Environ. Exp. Bot.*, 33(1), 99-119, DOI:
650 10.1016/0098-8472(93)90059-o, 1993.

651 Khan, T. R., Obrist, D., Agnan, Y., Selin, N. E., and Perlinger, J. A.: Atmosphere-terrestrial
652 exchange of gaseous elemental mercury: parameterization improvement through direct comparison
653 with measured ecosystem fluxes, *Environ. Sci. Process. Impacts*, 21(10), 1699-1712, DOI:
654 10.1039/C9EM00341J, 2019.

655 Laacouri, A., Nater, E. A., and Kolka, R. K.: Distribution and uptake dynamics of mercury in leaves
656 of common deciduous tree species in Minnesota, USA, *Environ. Sci Technol.*, 47(18), 10462-10470,



- 657 DOI: 10.1021/es401357z, 2013.
- 658 Lin, C. J., and Pehkonen, S. O.: The chemistry of atmospheric mercury: a review, *Atmos. Environ.*,
659 33(13), 2067-2079, DOI: 10.1016/S1352-2310(98)00387-2, 1999.
- 660 Lindberg, S. E., Jackson, D. R., Huckabee, J. W., Janzen, S. A., Levin, M. J., and Lund, J. R.:
661 Atmospheric emission and plant uptake of mercury from agricultural soils near the Almaden mercury
662 mine, *J. Environ. Qual.*, 8(4), 572-578, DOI: 10.2134/jeq1979.00472425000800040026x, 1979.
- 663 Lindberg, S., Bullock, R., Ebinghaus, R., Engstrom, D., Feng, X., Fitzgerald, W., Pirrone, N.,
664 Prestbo, E., and Seigneur, C.: A synthesis of progress and uncertainties in attributing the sources of
665 mercury in deposition, *Ambio*, 36(1), 19-32, <http://www.jstor.org/stable/4315781>, 2007.
- 666 Liu, Y., Lin, C. J., Yuan, W., Lu, Z., and Feng, X.: Translocation and distribution of mercury in
667 biomasses from subtropical forest ecosystems: Evidence from stable mercury isotopes, *Acta*
668 *Geochim.*, 40(1), 42-50, DOI: 10.1007/s11631-020-00441-3, 2021.
- 669 Mao, H., and Talbot, R.: Speciated mercury at marine, coastal, and inland sites in New England–
670 Part 1: Temporal variability, *Atmos. Chem. Phys.*, 12(11), 5099-5112, DOI: 10.5194/acp-12-5099-
671 2012, 2012.
- 672 McLagan, D. S., Monaci, F., Huang, H., Lei, Y. D., Mitchell, C. P. J., and Wania, F.:
673 Characterization and quantification of atmospheric mercury sources using passive air samplers. *J.*
674 *Geophys. Res. Atmos.*, 124(4), 2351-2362, DOI: 10.1029/2018JD029373, 2019.
- 675 McLagan, D. S., Stupple, G. W., Darlington, A., Hayden, K., and Steffen, A.: Where there is smoke
676 there is mercury: Assessing boreal forest fire mercury emissions using aircraft and highlighting
677 uncertainties associated with upscaling emissions estimates, *Atmos. Chem. Phys.*, 21(7), 5635-5653,
678 DOI: 10.5194/acp-21-5635-2021, 2021a.
- 679 McLagan, D. S., Osterwalder, S., and Biester, H.: Temporal and spatial assessment of gaseous
680 elemental mercury concentrations and emissions at contaminated sites using active and passive
681 measurements, *Environ. Res. Commun.*, 3(5), p.051004, DOI: 10.1088/2515-7620/abfe02/meta,
682 2021b.
- 683 McLagan, D. S., Schwab, L., Wiederhold, J. G., Chen, L., Pietrucha, J., Kraemer, S. M., and Biester,
684 H.: Demystifying mercury geochemistry in contaminated soil–groundwater systems with
685 complementary mercury stable isotope, concentration, and speciation analyses, *Environ. Sci. Process.*
686 *Impacts*, DOI: 10.1039/D1EM00368B, 2022.



687 Metsä-Kortelainen, S., Antikainen, T., and Viitaniemi, P.: The water absorption of sapwood and
688 heartwood of Scots pine and Norway spruce heat-treated at 170 C, 190 C, 210 C and 230 C, *Holz als*
689 *Roh-und Werkstoff*, 64(3), 192-197, DOI: 10.1007/s00107-005-0063-y, 2006.

690 Millhollen, A. G., Gustin, M. S., and Obrist, D.: Foliar mercury accumulation and exchange for
691 three tree species, *Environ. Sci Technol.*, 40(19), 6001-6006, DOI: 10.1021/es0609194, 2006.

692 Moreno, F. N., Anderson, C. W., Stewart, R. B., Robinson, B. H., Ghomshei, M., and Meech, J. A.:
693 Induced plant uptake and transport of mercury in the presence of sulphur-containing ligands and
694 humic acid. *New Phytol.*, 166(2), 445-454, DOI: 10.1111/j.1469-8137.2005.01361.x, 2005.

695 Moreno-Jiménez, E., Gamarra, R., Carpena-Ruiz, R. O., Millán, R., Peñalosa, J. M., and Esteban,
696 E.: Mercury bioaccumulation and phytotoxicity in two wild plant species of Almadén area,
697 *Chemosphere*, 63(11), 1969-1973, DOI: 10.1016/j.chemosphere.2005.09.043, 2006.

698 Mowat, L. D., St. Louis, V. L., Graydon, J. A., and Lehnher, I.: Influence of forest canopies on the
699 deposition of methylmercury to boreal ecosystem watersheds, *Environ. Sci Technol.*, 45(12), 5178-
700 5185, DOI: 10.1021/es104377y, 2011.

701 Nagy, N. E., Sikora, K., Krokene, P., Hietala, A. M., Solheim, H., and Fossdal, C. G.: Using laser
702 micro-dissection and qRT-PCR to analyze cell type-specific gene expression in Norway spruce
703 phloem, *PeerJ*, 2, e362, DOI: 10.7717/peerj.362, 2014.

704 Navrátil, T., Šimeček, M., Shanley, J. B., Rohovec, J., Hojdová, M., and Houška, J.: The history of
705 mercury pollution near the Spolana chlor-alkali plant (Neratovice, Czech Republic) as recorded by
706 Scots pine tree rings and other bioindicators, *Sci. Total Environ.*, 586, 1182-1192, DOI:
707 10.1016/j.scitotenv.2017.02.112, 2017.

708 Navrátil, T., Nováková, T., Shanley, J. B., Rohovec, J., Matoušková, S., Vaňková, M., and Norton,
709 S. A.: Larch tree rings as a tool for reconstructing 20th century Central European atmospheric
710 mercury trends, *Environ. Sci Technol.*, 52(19), 11060-11068, DOI: 10.1021/acs.est.8b02117, 2018.

711 Nováková, T., Navrátil, T., Demers, J. D., Roll, M., and Rohovec, J.: Contrasting tree ring Hg
712 records in two conifer species: Multi-site evidence of species-specific radial translocation effects in
713 Scots pine versus European larch, *Sci. Total Environ.*, 762, 144022, DOI:
714 10.1016/j.scitotenv.2020.144022, 2021.

715 Nováková T., Navrátil T., Schütze M., Rohovec J., Matoušková Š., Hošek M., Matys Grygar T.:
716 Reconstructing atmospheric Hg levels near the oldest chemical factory in central Europe using a tree
717 ring archive, *Environ. Pollut.*, 304, 119215, DOI: 10.1016/j.envpol.2022.119215, 2022.



718 Obrist, D., Agnan, Y., Jiskra, M., Olson, C. L., Colegrove, D. P., Hueber, J., Moore, C. W., Sonke,
719 J. E., and Helmig, D.: Tundra uptake of atmospheric elemental mercury drives Arctic mercury
720 pollution, *Nature*, 547(7662), 201-204, DOI: 10.1038/nature22997, 2017.

721 Obrist, D., Kirk, J. L., Zhang, L., Sunderland, E. M., Jiskra, M., and Selin, N. E.: A review of global
722 environmental mercury processes in response to human and natural perturbations: Changes of
723 emissions, climate, and land use, *Ambio*, 47(2), 116-140, DOI: 10.1007/s13280-017-1004-9, 2018.

724 Odabasi, M., Tolunay, D., Kara, M., Falay, E. O., Tuna, G., Altioek, H., Dumanoglu, Y., Bayram,
725 A., and Elbir, T.: Investigation of spatial and historical variations of air pollution around an industrial
726 region using trace and macro elements in tree components, *Sci. Total Environ.*, 550, 1010-1021, DOI:
727 10.1016/j.scitotenv.2016.01.197, 2016.

728 O'Connor, D., Hou, D., Ok, Y. S., Mulder, J., Duan, L., Wu, Q., Wang, S., Tack, F. M., and
729 Rinklebe, J.: Mercury speciation, transformation, and transportation in soils, atmospheric flux, and
730 implications for risk management: A critical review, *Environ. Int.*, 126, 747-761, DOI:
731 10.1016/j.envint.2019.03.019, 2019.

732 Peckham, M. A., Gustin, M. S., Weisberg, P. J., and Weiss-Penzias, P.: Results of a controlled field
733 experiment to assess the use of tree tissue concentrations as bioindicators of air Hg, *Biogeochem.*,
734 142(2), 265-279, DOI: 10.1007/s10533-018-0533-z, 2019a.

735 Peckham, M. A., Gustin, M. S., and Weisberg, P. J.: Assessment of the suitability of tree rings as
736 archives of global and regional atmospheric mercury pollution, *Environ. Sci Technol.*, 53(7), 3663-
737 3671, DOI: 10.1021/acs.est.8b06786, 2019b.

738 Peralta-Videa, J. R., Lopez, M. L., Narayan, M., Saupe, G., and Gardea-Torresdey, J.: The
739 biochemistry of environmental heavy metal uptake by plants: implications for the food chain, *Int. J.*
740 *Biochem. Cell Biol.*, 41(8-9), 1665-1677, DOI: 10.1016/j.biocel.2009.03.005, 2009.

741 Pfautsch, S., Hölttä, T., and Mencuccini, M.: Hydraulic functioning of tree stems—fusing ray
742 anatomy, radial transfer and capacitance, *Tree Physiol.*, 35(7), 706-722, DOI:
743 10.1093/treephys/tpv058, 2015.

744 Rea, A. W., Lindberg, S. E., and Keeler, G. J.: Assessment of dry deposition and foliar leaching of
745 mercury and selected trace elements based on washed foliar and surrogate surfaces. *Environ. Sci*
746 *Technol.*, 34(12), 2418-2425, DOI: 10.1021/es991305k, 2000.

747 Rea, A. W., Lindberg, S. E., and Keeler, G. J.: Dry deposition and foliar leaching of mercury and
748 selected trace elements in deciduous forest throughfall. *Atmos. Environ.*, 35(20), 3453-3462, DOI:



- 749 10.1016/S1352-2310(01)00133-9, 2001.
- 750 Rea, A. W., Lindberg, S. E., Scherbatskoy, T., and Keeler, G. J.: Mercury accumulation in foliage
751 over time in two northern mixed-hardwood forests. *Water Air Soil Pollut.*, 133(1), 49-67, DOI:
752 10.1023/A:1012919731598, 2002.
- 753 Richard, J. H., Bischoff, C., Ahrens, C. G., and Biester, H.: Mercury (II) reduction and co-
754 precipitation of metallic mercury on hydrous ferric oxide in contaminated groundwater, *Sci. Total*
755 *Environ.*, 539, 36-44, DOI: 10.1016/j.scitotenv.2015.08.116, 2016.
- 756 Scanlon, T. M., Riscassi, A. L., Demers, J. D., Camper, T. D., Lee, T. R., and Druckenbrod, D. L.:
757 Mercury accumulation in tree rings: observed trends in quantity and isotopic composition in
758 Shenandoah National Park, Virginia, *J. Geophys. Res. Biogeosci.*, 125(2), p.e2019JG005445, DOI:
759 10.1029/2019JG005445, 2020.
- 760 Schrenk, V., and Hiester, U.: Analysis of Subsurface Remediation Technologies for Brownfield
761 Redevelopments, REVIT: revitalising industrial sites, City of Stuttgart, Stuttgart, Germany,
762 P042/0702, 97. [https://www.researchgate.net/publication/283082200_Analysis_of_Subsurface](https://www.researchgate.net/publication/283082200_Analysis_of_Subsurface_Remediation_Technologies_for_Brownfield_Redevelopments)
763 [_Remediation_Technologies_for_Brownfield_Redevelopments](https://www.researchgate.net/publication/283082200_Analysis_of_Subsurface_Remediation_Technologies_for_Brownfield_Redevelopments), 2007.
- 764 Schroeder, W. H., and Munthe, J.: Atmospheric mercury—an overview. *Atmos. Environ.*, 32(5),
765 809-822, DOI: 10.1016/S1352-2310(97)00293-8, 1998.
- 766 Selin, N. E.: Global biogeochemical cycling of mercury: a review, *Annu. Rev. Environ. Resour.*,
767 34, 43-63, DOI: 10.1146/annurev.environ.051308.084314, 2009.
- 768 Selin, N. E., Jacob, D. J., Yantosca, R. M., Strode, S., Jaeglé, L., and Sunderland, E. M.: Global 3-
769 D land-ocean-atmosphere model for mercury: Present-day versus preindustrial cycles and
770 anthropogenic enrichment factors for deposition, *Global Biogeochem. Cy.*, 22(2), GB2011, DOI:
771 10.1029/2007GB003040, 2008.
- 772 Siwik, E. I., Campbell, L. M., and Mierle, G.: Distribution and trends of mercury in deciduous tree
773 cores, *Environ. Pollut.*, 158(6), 2067-2073, DOI: 10.1016/j.envpol.2010.03.002, 2010.
- 774 Sprovieri, F., Pirrone, N., Bencardino, M., D'Amore, F., Carbone, F., Cinnirella, S., Mannarino, V.,
775 Landis, M., Ebinghaus, R., Weigelt, A., Brunke, E.G., Labuschagne, C., Martin, L., Munthe, J.,
776 Wängberg, I., Artaxo, P., Morais, F., de Melo Jorge Barbosa, H., Brito, J., Cairns, W., Barbante, C.,
777 del Carmen Diéguez, M., Garcia P. E., Dommergue, A., Angot, H., Magand, O., Skov, H., Horvat,
778 M., Kotnik, J., Read, K. A., Mendes Neves, L., Gawlik, B. M., Sena, F., Mashyanov, N., Obolkin,
779 V., Wip, D., Feng, X. B., Zhang, H., Fu, X., Ramachandran, R., Cossa, D., Knoery, J., Maruszczak,



780 N., Nerentorp, M., and Norstrom C.: Atmospheric mercury concentrations observed at ground-based
781 monitoring sites globally distributed in the framework of the GMOS network, *Atmos. Chem. Phys.*,
782 16(18), 11915-11935, DOI: 10.5194/acp-16-11915-2016, 2016.

783 Sun, R., Streets, D. G., Horowitz, H. M., Amos, H. M., Liu, G., Perrot, V., Toutain, J. P.,
784 Hintelmann, H., Sunderland, E. M., Sonke, J. E., and Blum, J. D.: Historical (1850–2010) mercury
785 stable isotope inventory from anthropogenic sources to the atmosphere. *Elementa Sci. Anthropocene*,
786 2016, 4, 91.

787 Szponar, N., McLagan, D. S., Kaplan, R. J., Mitchell, C. P., Wania, F., Steffen, A., Stuppel, G. W.,
788 Monaci, F., and Bergquist, B. A.: Isotopic characterization of atmospheric gaseous elemental mercury
789 by passive air sampling, *Environ. Sci. Technol.*, 54(17), 10533-10543, DOI:
790 10.12952/journal.elementa.000091, 2020.

791 Taylor, A. M., Gartner, B. L., and Morrell, J. J.: Heartwood formation and natural durability-a
792 review. *Wood Fibre Sci.*, 2002, 34(4), 587-611.

793 Wang, X., Luo, J., Yin, R., Yuan, W., Lin, C.J., Sommar, J., Feng, X., Wang, H., and Lin, C.: Using
794 mercury isotopes to understand mercury accumulation in the montane forest floor of the Eastern
795 Tibetan Plateau. *Environ. Sci. Technol.*, 2017, 51(2), 801-809.

796 Wang, X., Yuan, W., Lin, C. J., Luo, J., Wang, F., Feng, X., Fu, X., and Liu, C.: Underestimated
797 sink of atmospheric mercury in a deglaciated forest chronosequence, *Environ. Sci. Technol.*, 54(13),
798 8083-8093, DOI: 10.1021/acs.est.0c01667, 2020.

799 Wang, X., Yuan, W., Lin, C. J., Wu, F., and Feng, X.: Stable mercury isotopes stored in Masson
800 Pinus tree rings as atmospheric mercury archives, *J. Hazard. Mater.*, 415, 125678, DOI:
801 10.1016/j.jhazmat.2021.125678, 2021.

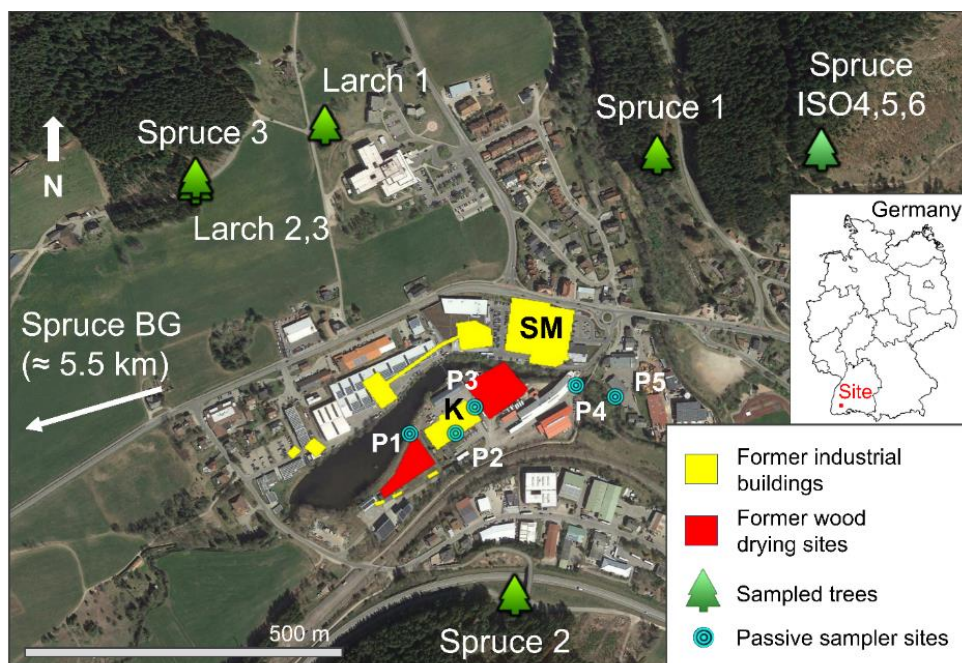
802 Weis, R.: Vor 100 Jahren brannte in Titisee-Neustadt das Dampfsäge- und Holzwerk Himmelsbach,
803 *Badische Zeitung BZ*, [https://www.badische-zeitung.de/vor-100-jahren-brannte-in-titisee-neustadt-
804 das-dampfsaegel-und-holzwerk-himmelsbach--188906523.html](https://www.badische-zeitung.de/vor-100-jahren-brannte-in-titisee-neustadt-das-dampfsaegel-und-holzwerk-himmelsbach--188906523.html), 2020.

805 Wiederhold, J. G., Christopher J. C., Daniel, K., Infante, I., Bourdon D., and Kretzschmar, R.:
806 Equilibrium Mercury Isotope Fractionation between Dissolved Hg(II) Species and Thiol-Bound Hg,
807 *Environ. Sci. Technol.*, 44(11), 4191–4197, DOI:10.1021/es100205t, 2010.

808 Wohlgenuth, L., Osterwalder, S., Joseph, C., Kahmen, A., Hoch, G., Alewell, C., and Jiskra, M.:
809 A bottom-up quantification of foliar mercury uptake fluxes across Europe, *Biogeosci.*, 17(24), 6441-
810 6456, DOI: 10.5194/bg-17-6441-2020, 2020.



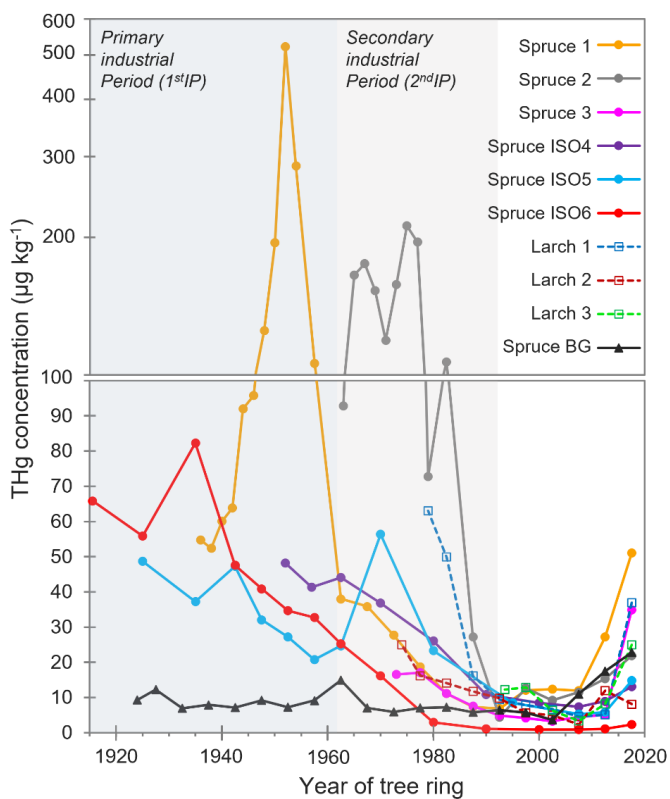
- 811 Wright, G., Woodward, C., Peri, L., Weisberg, P. J., and Gustin, M. S.: Application of tree rings
812 [dendrochemistry] for detecting historical trends in air Hg concentrations across multiple scales.
813 *Biogeochem.*, 120(1), 149-162, DOI: 10.1007/s10533-014-9987-9, 2014.
- 814 Yamakawa, A., Amouroux, D., Tessier, E., Bérail, S., Fettig, I., Barre, J.P., Koschorreck, J., Rüdél,
815 H., and Donard, O.F.: Hg isotopic composition of one-year-old spruce shoots: Application to long-
816 term Hg atmospheric monitoring in Germany, *Chemosphere*, 279, 130631, DOI:
817 10.1016/j.chemosphere.2021.130631, 2021.
- 818 Yanai, R. D., Yang, Y., Wild, A. D., Smith, K. T., and Driscoll, C. T.: New Approaches to
819 Understand Mercury in Trees: Radial and Longitudinal Patterns of Mercury in Tree Rings and
820 Genetic Control of Mercury in Maple Sap, *Water Air Soil Pollut.*, 231, 1-10, DOI: 10.1007/s11270-
821 020-04601-2, 2020.
- 822 York, D., Evensen, N. M., Martinez, M. L., and De Basabe Delgado, J.: Unified equations for the
823 slope, intercept, and standard errors of the best straight line, *Am. J. Phys.*, 72(3), 367-375, DOI:
824 10.1119/1.1632486, 2004.
- 825 Yuan, W., Sommar, J., Lin, C. J., Wang, X., Li, K., Liu, Y., Zhang, H., Lu, Z., Wu, C., and Feng,
826 X.: Stable isotope evidence shows re-emission of elemental mercury vapor occurring after reductive
827 loss from foliage, *Environ. Sci Technol.*, 53(2), 651-660, DOI: 10.1021/acs.est.8b04865, 2018.
- 828 Zhang, L., Wright, L. P., and Blanchard, P.: A review of current knowledge concerning dry
829 deposition of atmospheric mercury, *Atmos. Environ.*, 43(37), 5853-5864, DOI:
830 10.1016/j.atmosenv.2009.08.019, 2009.
- 831 Zheng, W., and Hintelmann, H.: Mercury isotope fractionation during photoreduction in natural
832 water is controlled by its Hg/DOC ratio, *Geochim. Cosmochim. Acta*, 73(22), 6704-6715, DOI:
833 10.1016/j.gca.2009.08.016, 2009.
- 834 Zhou, J., Wang, Z., Zhang, X., and Gao, Y.: Mercury concentrations and pools in four adjacent
835 coniferous and deciduous upland forests in Beijing, China, *J. Geophys. Res. Biogeosci.*, 122(5), 1260-
836 1274, DOI: 10.1002/2017JG003776, 2017.
- 837



838

839 *Figure 1: Map showing the location of sampled trees, former industrial buildings and wood drying*
840 *sites (before 1968), and passive sampler locations (labelled P1–P5). The location of spruce*
841 *background tree (spruce BG) is ≈5.5 kilometres west southwest of the study site (direction indicated*
842 *on map). SM – Former sawmill; K – former kyanisation hall/wood treatment area. The three spruce*
843 *ISO trees are from the deforested stand in the northwest of Fig. 1; exact location of each of these*
844 *trees within this stand is unknown (trees felled by forest workers). ©Google Earth 2019.*

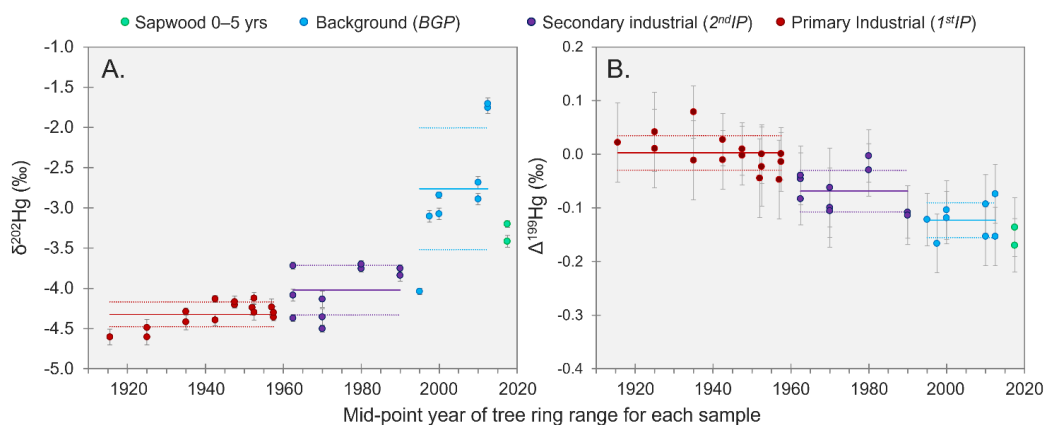
845



846

847 **Figure 2:** THg concentrations in tree rings dated by year. Years of tree rings correspond to the
848 middle point of samples of combined adjacent rings (i.e., 0–5 year = 2.5 years). Y-axis is split at 100
849 $\mu\text{g}\cdot\text{kg}^{-1}$ changing from normal- to log-scale due to the very high concentrations measured in Spruce
850 1 and Spruce 2. 1stIP (before 1962) and 2ndIP (1962–1992) are highlighted.

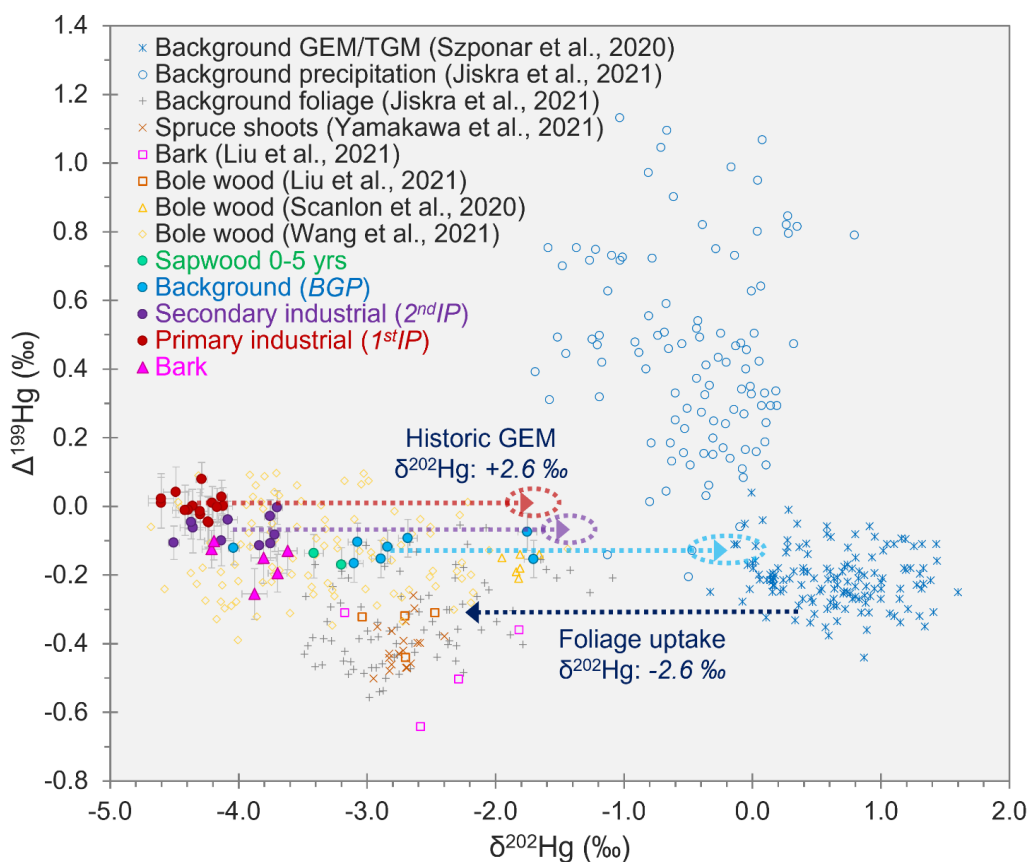
851



852

853 **Figure 3:** $\delta^{202}\text{Hg}$ (Panel A) and $\Delta^{199}\text{Hg}$ (Panel B) in tree rings dated by year for samples from
854 spruce ISO4–6 trees. Solid and dotted lines for each period represent the mean and standard
855 deviation, respectively. Data displayed are the composite of all three trees (figures for individual
856 trees are shown in Section S6). Data for THg plotted against MDF and THg against MIF are shown
857 in Section S7. Error bars for individual datapoints represent session 2SD for secondary standard
858 “ETH Fluka”.

859



860

861 **Figure 4:** Relationships between $\Delta^{199}\text{Hg}$ and $\delta^{202}\text{Hg}$ for tree rings samples from spruce ISO4–6
862 trees analysed for Hg stable isotopes (data with solid markers). Figure includes the $\Delta^{199}\text{Hg}$ and
863 $\delta^{202}\text{Hg}$ values for tree samples (bole wood, bark, foliage, and shoots) from other studies. Additionally,
864 background TGM/GEM data were included to show the $\approx -2.6 \text{‰}$ MDF associated with stomatal
865 uptake of GEM (dark blue dotted line), and background precipitation samples were included to
866 demonstrate that there was little influence from precipitation on found Hg in within trees. The red,
867 purple, and light-blue dotted lines indicate the predicted GEM values in air at the site during the
868 1stIP, 2ndIP, and BGP, respectively, based off the mean measured $\delta^{202}\text{Hg}$ values in tree rings for these
869 respective periods (MIF was assumed to be zero for stomatal uptake in these calculations).

870